

See discussions, stats, and author profiles for this publication at: <https://www.researchgate.net/publication/262876788>

Anisotropic Etching of Semiconductor Nanocrystals

ARTICLE *in* CHEMISTRY OF MATERIALS · NOVEMBER 2011

Impact Factor: 8.35 · DOI: 10.1021/cm202514a

CITATIONS

22

READS

56

4 AUTHORS, INCLUDING:



Sung Jun Lim

University of Illinois, Urbana-Champaign

14 PUBLICATIONS 175 CITATIONS

[SEE PROFILE](#)



Seung Koo Shin

Pohang University of Science and Technology

79 PUBLICATIONS 1,347 CITATIONS

[SEE PROFILE](#)

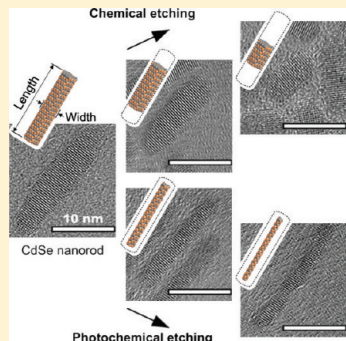
Anisotropic Etching of Semiconductor Nanocrystals

Sung Jun Lim, Wonjung Kim, Sunghan Jung, Jongcheol Seo, and Seung Koo Shin*

Bio-Nanotechnology Center, Department of Chemistry, Pohang University of Science and Technology, San 31, Hyoja-dong, Nam-gu, Pohang, Kyungbuk 790-784, Korea

 Supporting Information

ABSTRACT: The size and shape of CdSe nanorods, CdSe tetrapods, and CdS nanowires were tailored by chemical and photochemical etchings in chloromethane solvents. Nanocrystals were synthesized by colloidal growth, and their sizes and shapes were visualized by transmission electron microscopy before and after etching. Crystal structures were confirmed by X-ray diffraction, and optical properties were monitored during etching. Chemical etching with tributylphosphine preferentially shortens the length of nanocrystals, whereas photochemical etching with both primary alkylamine and tributylphosphine reduces the diameter more than the length. The surface of etched nanocrystals was characterized by X-ray photoelectron spectroscopy, and the etching products dissolved in solvent were analyzed by matrix-free laser desorption ionization mass spectrometry. Spectroscopic results suggest that the chloride ion is the active species: Chloride ions are generated either by chemical activation of chloromethane solvents with tributylphosphine or by photoinduced electron transfer from nanocrystals to chloromethane solvents adsorbed on the nanocrystal surface. Tributylphosphine increases the rate of both chemical and photochemical etching, whereas primary alkylamine inhibits chemical etching. Both chemical and photochemical etching processes can be combined together with organic-based colloidal synthesis to anisotropically reshape the quantum-size and aspect ratio of nanocrystals.



KEYWORDS: anisotropic nanocrystal etching, chemical etching, photochemical etching, facet-selective etching, quantum size-selective etching

INTRODUCTION

Colloidal semiconductor nanocrystals are produced in various sizes and shapes by solution-phase synthesis in organic solvents,^{1–8} and the novel quantum-confinement effects on their optical properties are widely used in optoelectronic applications.^{9,10} The size and shape of nanocrystals are typically controlled by colloidal growth conditions: The size-selective synthesis yields monodisperse, single-crystalline nanocrystals with wide size-tunability,^{1,2} whereas the shape-selective synthesis results in homocrystalline nanorods^{3–5} and nanowires,⁶ as well as heterocrystalline multipods^{5,7,8} with limited size-tunability, because the kinetic growths of anisotropic nanocrystals compromise size-focusing conditions.^{3–8} For instance, the kinetically grown nanorods or nanowires show significant spreads in size distribution as the aspect ratio increases, thus, their exciton absorption bands are much broader than those of highly monodisperse quantum dots.^{3–6} Thus, it is a challenge to produce anisotropic nanocrystals in a narrow size distribution, and there is a need for aligned assemblies of such materials in optoelectronic applications.^{9,10} To this end, we attempted the reshaping of anisotropic nanocrystals obtained from shape-selective syntheses, by means of chemical and/or photochemical etching. Herein, we present the length-selective chemical etching and the diameter-selective photochemical etching of anisotropic nanocrystals in chlorine-containing solvents compatible with organic-based colloidal synthesis.

To date, there have been a number of reports that demonstrate surface etching of semiconductor nanocrystal

quantum dots either by chemicals^{11–14} or by photoinduced processes.^{15–20} Chemicals dissolve surface atoms to round and trim the corners and edges of quantum dots.^{13,14} Photons induce photo-oxidation and dissolution of surface atoms.^{15–18} For instance, CdSe quantum dots emitting in the violet–blue region were prepared by the oxidation of red-emitting ones with hydrogen peroxide in water.¹¹ Blue-emitting CdTe quantum dots were also obtained by etching red-emitting ones with tetrafluoroborate in air-saturated water.¹² PbS quantum dots were reduced in both the size and the aspect ratio by etching with hydrochloric acid.¹³ On the other hand, photochemical etching reduced the average size of quantum dots, such as CdS,¹⁵ CdSe,^{16,19} CdTe,¹⁷ CdSe/ZnS,¹⁹ and InP,²⁰ as well as CdS nanorods.¹⁸ Most of the reported etching processes occur in water^{11–18} and are thus incompatible with organic-based synthesis. Moreover, the water-based etching requires water-soluble surface passivation of organic-soluble nanocrystals either with hydrophilic ligands¹⁴ or with a thick silica shell,^{16,18} in order to keep unpassivated nanocrystals from aggregation during etching. Further, the water-based chemical etching isotropically reduces the size and shape of nanocrystals.^{11–13,15–17} The anisotropic length- or diameter-selective etching has rarely been reported. Amine-assisted oxidative etching has been shown to be facet-selective on wurtzite CdSe

Received: August 23, 2011

Revised: October 13, 2011

Published: October 28, 2011

quantum dots, but it occurs too slowly to be practical.¹⁴ Photochemical oxidative etching has reduced both the length and diameter of silica-coated wurtzite CdS nanorods.¹⁸

To perform etching in combination with colloidal growths, we need to develop processes that are compatible with organic-based synthesis, that proceed at a controllable rate, and that allow easy control over the initiation and termination of the etching process. We find chemical and photochemical conditions for controllable nanocrystal etching in chlorine-containing solvents, which enable the length- and diameter-selective reduction of CdSe nanorods, CdSe tetrapods, and CdS nanowires. Chloroform or tetrachloromethane is used as a solvent because it not only dissolves organic-soluble nanocrystals but also can be easily removed after etching by evaporation. Tributylphosphine (TBP) is used as an additive because TBP is a good coordinating ligand for selenium and sulfur.²¹ Primary alkylamine is used as an inhibitor in chemical etching or as a coadditive in photochemical etching because primary amine is a good ligand for cadmium.²¹

Wurtzite (W) CdSe nanorods, zinc-blend (ZB) CdSe core/W CdSe arm tetrapods, and W CdS nanowires were prepared by colloidal syntheses and stored in anhydrous hexane under argon. The crystal structure was confirmed by powder X-ray diffraction (XRD). The size and shape distributions were measured by transmission electron microscopy (TEM) before and after etching. Optical properties were monitored during etching by UV-vis absorption and photoluminescence (PL) spectroscopy. In addition, the surface composition of nanocrystals was analyzed by X-ray photoelectron spectroscopy (XPS) before and after etching. The etching products dissolved in solvent were identified by mass spectrometry (MS). On the basis of XPS and MS results, a mechanism of chemical and photochemical etching in chloromethane solvents is proposed.

EXPERIMENTAL SECTION

Chemicals. Cadmium oxide (CdO, 99.99%) was purchased from Kojundo Chemical Laboratory (Saitama, Japan). Dodecylphosphonic acid (DDPA, 95%) and tetradecylphosphonic acid (TDPA, 98%) were purchased from Alfa Aesar (Ward Hill, MA). Sulfur powder (99.998%), selenium powder (100-mesh, ≥99.99%), tributylphosphine (TBP, 97%), trioctylphosphine (TOP, technical grade, 90%), triethylphosphine oxide (TBPO, 95%), triethylphosphine oxide (TOPO, 99%), propylamine (PA, 98%), butylamine (99.5%), octylamine (99%), oleylamine (OA, technical grade, 70%), oleic acid (technical grade, 90%), 1-octadecene (ODE, technical grade, 90%), cetyltrimethylammonium bromide (CTAB, ≥99%), chloroform (>99%, anhydrous), tetrachloromethane (≥99.5%, anhydrous), hexane (95%, anhydrous), and toluene (99.8%, anhydrous) were purchased from Sigma-Aldrich (St. Louis, MO). HPLC grade hexane, methanol, ethanol, and isopropanol were obtained from J. T. Baker (Phillipsburg, NJ). Both chloroform and tetrachloromethane were degassed by several freeze-pump-thaw cycles before use. All other chemicals were used without further purification. Mono-octylphosphinic acid (MOPA) was prepared according to the literature.²²

Nanocrystal Synthesis. CdSe nanorods and CdS nanowires were synthesized following the literature^{5,23,24} with some modification, whereas CdSe tetrapods were prepared using the method of Wong and colleagues.⁸

CdSe Nanorods (~22 nm × ~6 nm). A selenium stock solution (0.5 M) was prepared by dissolving selenium powder (1 mmol) in TBP (2 mL) by ~5 min sonication. A cadmium precursor solution was prepared by mixing CdO (1 mmol) with TDPA (2 mmol) in ODE (5 mL); the mixture was degassed at 120 °C for 10 min under vacuum and then heated to 330–340 °C under argon. When the solution was clear and colorless, we quickly injected the selenium stock solution (1 mL). The temperature was dropped to ~315 °C and held at 315 °C

for ~5 min. Then, the selenium stock solution (1 mL) was injected again, and the temperature was dropped to ~310 °C. The temperature was elevated to ~315 °C within ~1 min, and held at 315 °C for another 5 min. After cooling the solution temperature to <100 °C at bench, we added oleic acid (0.5–1 mL) mixed in hexane (HPLC grade, 20–25 mL) and washed the solution with methanol (HPLC grade, 20–30 mL) three times. The resulting CdSe nanorods (absorption band edge, $\lambda_{\text{abs}} = \sim 627$ nm) were harvested by precipitation in ethanol and stored in anhydrous hexane under argon.

CdSe Nanorods (~50 nm × ~8 nm). A selenium stock solution (0.5 M) was prepared by dissolving selenium powder (1 mmol) in TOP (2 mL) by ~5 min sonication. A cadmium precursor solution was prepared by mixing CdO (1 mmol) with DDPA (2 mmol) in TOPO (3.3 g); the mixture was degassed at 100 °C for 60 min under vacuum and then heated to ~310 °C under argon. When the solution was clear and colorless, we lowered the temperature to 280 °C and added MOPA (30 µL). Then, the selenium stock solution (0.5 mL) was injected four times every 2 min. The temperature was immediately dropped to ~270 °C after each injection, and it was raised back to ~280 °C within ~1 min. After the fourth injection, the temperature was held at ~280 °C for 5 min. After cooling the solution to <50 °C at bench, we added hexane (HPLC grade, 20–25 mL) and washed the precipitates with methanol (HPLC grade, 20–30 mL) twice. The resulting CdSe nanorods (absorption band edge, $\lambda_{\text{abs}} = \sim 642$ nm) were harvested by ethanol precipitation and stored in anhydrous hexane under argon.

CdSe Tetrapods. A selenium stock solution (0.33 M) was prepared by dissolving selenium powder (0.5 mmol) in TOP (1.5 mL) by ~5 min sonication. A cadmium precursor solution was prepared by mixing CdO (0.8 mmol) and oleic acid (10 mmol) in ODE (20 mL); the mixture was degassed at ~100 °C under vacuum for 10 min and then heated to 150 °C under argon. When the solution became transparent, we raised the temperature to 300 °C. The selenium stock solution mixed with CTAB (0.05 mmol) in anhydrous toluene (2 mL) was slowly injected into the cadmium precursor solution within 5–7 s. After the injection, the temperature was dropped to ~285 °C, and then the temperature was quenched within 1 min by removing heat and adding ODE (20 mL) stored at room temperature. After cooling the solution to <100 °C, we added hexane (HPLC grade, ~10 mL) and washed the solution three times with methanol (HPLC grade, 20–30 mL). The resulting CdSe tetrapods ($\lambda_{\text{abs}} = \sim 575$ nm) were harvested by ethanol precipitation and stored in anhydrous hexane under argon.

CdS Nanowires. A sulfur stock solution (~3.6 M) was prepared by dissolving sulfur powder (5.1 mmol) in TOP (1.4 mL) by vigorously stirring at ~200 °C until the solution became clear and yellow. A cadmium precursor solution was prepared by mixing CdO (1.55 mmol) with TDPA (3.1 mmol) in TOPO (3 g); the mixture was degassed at 120 °C for 30 min under vacuum and then heated to ~320 °C under argon. When the solution was clear and colorless, we added TOP (2 mL) and kept the temperature at ~315 °C. After the injection of the sulfur stock solution (1.4 mL), the temperature was dropped to ~305 °C and was held at ~305 °C for ~24 min. After cooling the solution to <100 °C, we added oleic acid (0.5–1 mL) mixed in hexane (HPLC grade, 20–25 mL) and washed the precipitates with isopropanol (HPLC grade, 20–30 mL) twice. The resulting CdS nanorods (absorption band edge, $\lambda_{\text{abs}} = \sim 480$ nm) were harvested by methanol precipitation and stored in anhydrous hexane under argon.

Chemical Etching. The etching solution was prepared in a 4-mL quartz cell under ambient conditions either by mixing TBP (100 µL) and TOPO (50 mg) in oxygen-free tetrachloromethane (3 mL) or by mixing TBP (200–300 µL) in oxygen-saturated chloroform (~3 mL). Oxygen-saturated chloroform was prepared by vigorously stirring chloroform under oxygen for ~30 min. TBP oxidation in oxygen-saturated chloroform was confirmed by the disappearance of the TBP absorption band at 244 nm in the UV-vis absorption spectra. CdSe and CdS nanocrystals (1–10 nmol) were dispersed in hexane (0.1–0.2 mL) and quickly injected into the etching solution at room temperature. The absorption spectra were monitored every 10–15 s for the tetrachloromethane solution and every 30–60 s for the

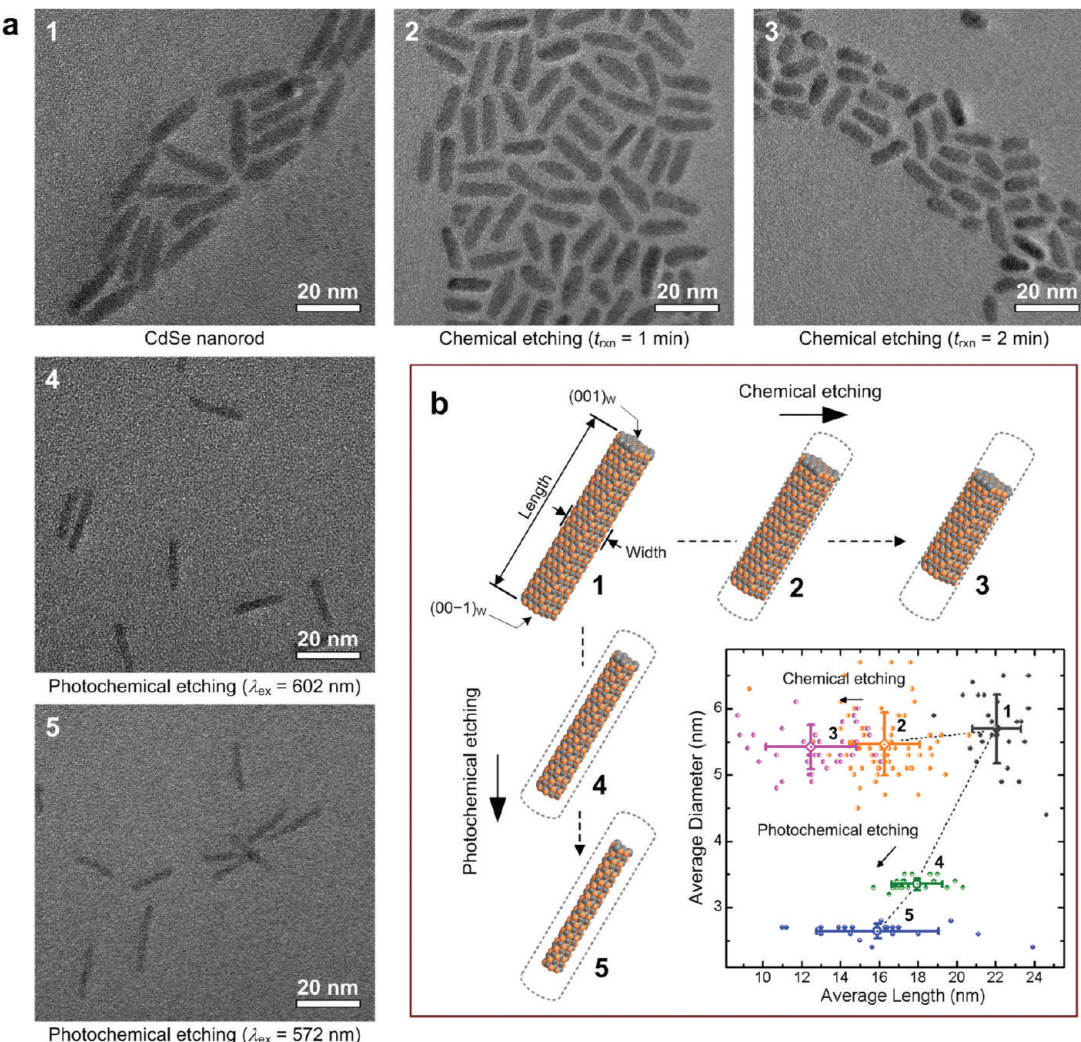


Figure 1. (a) TEM image of CdSe nanorods before (1) and after chemical (2, 3) or photochemical (4, 5) etching in oxygen-free tetrachloromethane. (b) Pictorial view of the shape change in the CdSe nanorod having a wurtzite (W) crystal structure; cadmium (gray), selenium (orange). $(001)_w$ and $(00-1)_w$ are the end planes perpendicular to the c -axis. The inset shows the average size (with error bars) and scattered size distribution of CdSe nanorods before and after etching.

chloroform solution. The etching reaction was quenched by the addition of PA ($500\text{ }\mu\text{L}$) within 1–2 min for the tetrachloromethane solution and within ~20 min for the chloroform solution. The resulting nanocrystals from etching were precipitated with methanol (30 mL) and kept in anhydrous hexane under argon.

Photochemical Etching. Either an Nd:YAG-pumped optical parametric oscillator (OPO) laser (Continuum, Powerlite 8000, and Sunlite OPO, Santa Clara, CA) or a hand-held UV lamp (UVGL-58, Upland, CA) was used as the excitation light source. CdSe and CdS nanocrystals (1–10 nmol) were dispersed under argon in a 4-mL quartz cell either containing oxygen-free tetrachloromethane (3 mL) with PA (200–300 μL), oleylamine (200–300 μL), and TBP (100 μL), or containing oxygen-free chloroform (3 mL) with PA (200 μL) and TBP (100 μL). PA was added before TBP to prevent any chemical etching. The mixture was magnetically stirred and irradiated with light either using an OPO laser (12 mm laser beam diameter, 10 mJ per pulse, 10 Hz repetition rate in the range 463–625 nm), or using a 254-nm UV lamp. For sequential chemical and photochemical etching, CdSe nanocrystals (1–10 nmol) were chemically etched first in oxygen-free tetrachloromethane with TBP and TOPO, and then quenched with PA ($500\text{ }\mu\text{L}$) within 1 min. After addition of oleylamine (300 μL), the mixture was irradiated with the OPO laser (625 nm) while stirring the solution. The absorption spectra were monitored either every 3–5 min for the chloroform solution under UV irradiation

or every 20–30 min for the tetrachloromethane solution under OPO laser irradiation. For the emission and PL decay measurements, an aliquot (200–300 μL) was diluted in chloroform (2 mL) with octylamine (200 μL) in a separate 4-mL quartz cell. The resulting nanocrystals from etching were precipitated with methanol (30 mL) containing oleic acid (<0.1 mL). The recovered nanocrystals were dispersed in hexane (2–3 mL) with OA (<0.1 mL), precipitated with methanol (10–15 mL), and kept in anhydrous hexane under argon.

Absorption and PL Spectroscopy. A diluted nanocrystal solution (0.05–0.1 in band-edge absorbance) in chloroform was prepared for optical characterization. The UV-vis absorption spectra were taken using an Agilent 8453 spectrometer (Santa Clara, CA). The emission spectra and PL decay were measured using a home-built bifurcated optical setup described in detail elsewhere.²¹ In brief, a nanocrystal sample was excited at 407 nm using a picosecond laser operating at 2.5 MHz with 35 pJ per pulse. The emission spectra were taken with a spectrograph equipped with a liquid-nitrogen-cooled charge-coupled device. The PL decay was monitored using a monochromator coupled to a photomultiplier tube (PMT). Both the signal from a single-photon counting PMT and the trigger from a laser pulse driver were sent to a reverse start-stop single photon counting module to record the time delay.

TEM. The size and shape of CdSe nanocrystals were visualized by TEM. A drop of a diluted CdSe nanocrystal solution in hexane was

Table 1. Average Size of CdSe Nanorods before and after Chemical or Photochemical Etching in Oxygen-Free Tetrachloromethane^a

	before etching	chemical etching		photochemical etching	
		$t_{\text{rxn}} = 1 \text{ min}$	$t_{\text{rxn}} = 2 \text{ min}$	$\lambda_{\text{ex}} = 602 \text{ nm}$	$\lambda_{\text{ex}} = 572 \text{ nm}$
aspect ratio ^b	3.9 ± 0.4	3.0 ± 0.4	2.3 ± 0.4	5.3 ± 0.4	6.1 ± 1.2
length ^b (L , nm)	22.0 ± 1.3	16.3 ± 1.8	12.5 ± 2.3	17.9 ± 1.3	15.9 ± 3.1
diameter ^b (ϕ , nm)	5.7 ± 0.5	5.5 ± 0.5	5.4 ± 0.3	3.4 ± 0.1	2.6 ± 0.1
ΔL (nm)	0	-5.7	-9.5	-4.1	-6.1
$\Delta\phi$ (nm)	0	-0.2	-0.3	-2.3	-3.1

^aThe numbers of nanorod samples are 26 (before etching), 67 (after 1-min chemical etching), 41 (after 2-min chemical etching), 23 (after 602-nm photochemical etching), and 20 (after 572-nm photochemical etching). ^bAn error denotes the standard deviation.

placed onto a 400-mesh copper grid with a carbon supporting film (Ted Pella, product no. 01824, Redding, CA). Excess liquid was wicked away, and it was dried under vacuum for >30 min. High-resolution TEM images were obtained with a FEI Tecnai G2 F30 TEM (Hillsboro, OR) operating at 300 keV. Normal TEM images were taken with a JEOL JEM-1011 (Tokyo, Japan) operating at 80 keV.

XRD. The crystal structure was analyzed by XRD. A drop of a nanocrystal solution in hexane was dried on a $1 \times 1 \text{ cm}^2$ silicon wafer. XRD patterns were obtained using a Rigaku D/MAX-2500 diffractometer (Tokyo, Japan).

XPS. The chemical composition of nanocrystal surface was characterized by XPS. A drop of nanocrystal solution in hexane was placed on a $1 \times 1 \text{ cm}^2$ silicon wafer coated with a 200-nm-thick gold layer and dried overnight under vacuum. The XPS spectra were taken using a Thermo Scientific K-Alpha XPS instrument (Waltham, MA) equipped with an Al $K\alpha$ radiation source. An area of $\sim 0.4 \text{ mm}$ in diameter was exposed to X-ray radiation. The XPS spectra were obtained by single scan over a 0–1350 eV range in 1 eV step and 50 ms dwell time per step with 200 eV pass energy. The XPS spectra were calibrated against the Au 4f peak and/or the C 1s peak.

MS. Etching products were further analyzed by matrix-free laser desorption ionization (LDI) MS. A completely etched product solution was prepared either by increasing the reaction time of chemical etching or by irradiating the photochemical etching solution with 254-nm UV until all nanocrystal peaks disappeared from the absorption spectra. Several drops of the etching product solution were loaded on a stainless steel target plate without matrix and dried under nitrogen flow. The mass spectra were acquired using a Bruker Reflex III time-of-flight mass spectrometer (Bremen, Germany) equipped with a 337-nm nitrogen laser. Each mass spectrum was obtained by accumulating 50 laser shots.

RESULTS AND DISCUSSION

Anisotropic Etching of CdSe Nanorods. Results from CdSe nanorod etching in oxygen-free tetrachloromethane are summarized in Figure 1. Chemical etching was carried out in the presence of TBP and TOPO, whereas photochemical etching was performed under OPO laser light in the presence of TBP, PA, and OA. TEM images show the morphology of nanocrystals before etching (Figure 1a-1), after 1 and 2 min chemical etching (parts a-2 and a-3 of Figure 1, respectively), and after photochemical etching at $\lambda_{\text{ex}} = 602$ and 572 nm (parts a-4 and a-5 of Figure 1, respectively). The average sizes (length and diameter) and aspect ratios obtained from TEM images are summarized in Table 1. Variations of average length and diameter of nanorods are illustrated in Figure 1b. W CdSe nanorods are truncated, with $(001)_W$ and $(00-1)_W$ facets at the ends of the c -axis. Chemical etching reduces the length of nanorod but induces no change in diameter, whereas photochemical etching narrows the diameter and shortens the length. The aspect ratio decreases from 3.9 to 3.0 and to 2.3 after 1 and 2 min of chemical etching, respectively, but

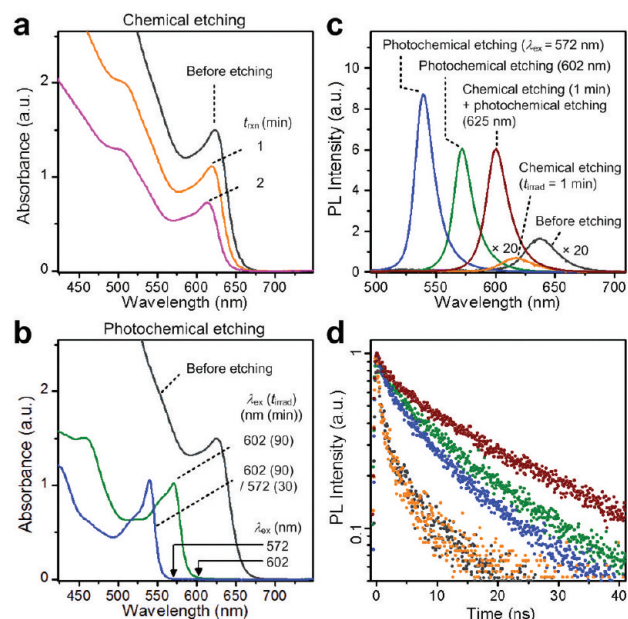


Figure 2. Absorption spectra of CdSe nanorods (a) before ($\lambda_{\text{abs}} = 623$ nm, black) and after chemical etching ($\lambda_{\text{abs}} = 619$ nm after 1 min, orange; $\lambda_{\text{abs}} = 614$ nm after 2 min, magenta) and (b) after photochemical etching ($\lambda_{\text{abs}} = 571$ nm after 90 min irradiation at $\lambda_{\text{ex}} = 602$ nm, olive; $\lambda_{\text{abs}} = 540$ nm after another 30 min irradiation at $\lambda_{\text{ex}} = 572$ nm, blue). (c) Emission spectra and (d) photoluminescence (PL) decay profile of CdSe nanorods before and after the etching shown in (a) and (b). Those of CdSe nanorods after 1-min chemical etching followed by photochemical etching for 50 min at $\lambda_{\text{ex}} = 625$ nm are also shown (brown). PL decay was measured at the emission maximum (λ_{em}). Optical properties (λ_{em} , fwhm, QE, and τ_{eff}) are listed in Table 2. a.u., arbitrary unit.

increases from 3.9 to 5.3 and to 6.1 after photochemical etching at 602 and 572 nm, respectively. The ratio of the change in length to the change in diameter ($\Delta L/\Delta\phi$) is ~ 30 for chemical etching and ~ 2 for photochemical etching, manifesting the remarkable anisotropy in etching: the length-selective chemical etching and the diameter-selective photochemical etching.

Similar anisotropic etching was observed from both chemical and photochemical etching in chloroform (see Figure S1 and Table S1 in the Supporting Information). Interestingly, nanorods remain intact in the absence of either oxygen or TBP. Moreover, no etching occurs on nanorods in the presence of phosphine oxide (TBPO or TOPO). Thus, it is evident that the addition of TBP in oxygen-saturated chloroform induces etching.

Optical Properties of Etched Nanorods. The absorption and emission spectra, as well as the PL decay profiles of

Table 2. Optical Properties of CdSe Nanorods before and after Chemical or Photochemical Etching in Tetrachloromethane Shown in Figure 2c and d

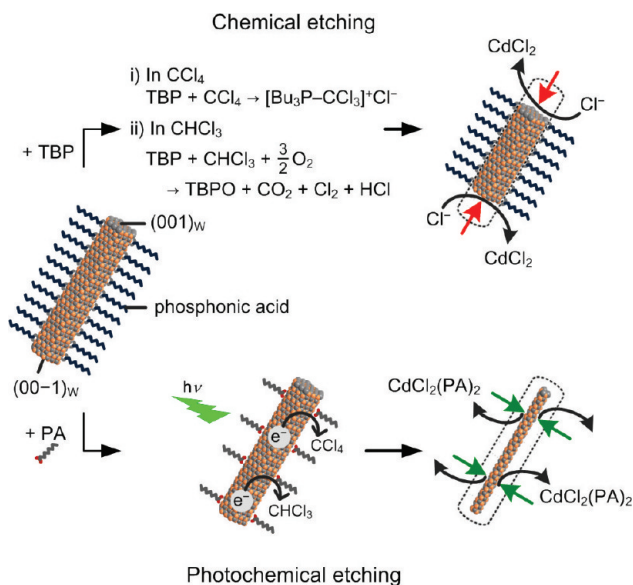
	λ_{abs} (nm)	λ_{em} (nm)	fwhm ^b (nm)	QE ^c (%)	τ_{eff}^d (ns)
before etching	623	637	32	0.7	0.55
chemical etching for 1 min ^a	607	618	30	0.3	0.33
chemical etching for 1 min + photochemical etching for 50 min at $\lambda_{\text{ex}} = 625 \text{ nm}^a$	592	601	22	37	11.8
photochemical etching for 90 min at $\lambda_{\text{ex}} = 602 \text{ nm}^a$	565	572	21	36	7.5
photochemical etching for 30 min at $\lambda_{\text{ex}} = 572 \text{ nm}^a$	533	539	19	56	6.0

^aOptical properties were measured after binary amine–phosphine passivation.²¹ ^bFull width at half-maximum (fwhm) of emission.

^cPhotoluminescence quantum efficiency (QE) is relative to rhodamine 101 in ethanol (QE = 100%). ^dEffective lifetime (τ_{eff}) (fitting parameters are listed in Table S2 in the Supporting Information).

CdSe nanorods, are shown in Figure 2. Characteristic absorption and emission wavelengths ($\lambda_{\text{abs}}/\lambda_{\text{em}}$), the full width at half-maximum (fwhm) of emission, the PL quantum efficiency (QE), and the PL lifetime (τ_{eff}) are listed in Table 2. Chemical etching in oxygen-free tetrachloromethane for 1 and 2 min gradually reduced the absorbance with slight blue-shift in band edge by 4 and 9 nm, respectively (Figure 2a), whereas photochemical etching in oxygen-free tetrachloromethane at $\lambda_{\text{ex}} = 602$ and 572 nm sharply reduced the absorbance and shifted band-edge to the blue by 55 and 83 nm, respectively (Figure 2b). Apparently, chemical etching decreases the absorption volume with little change in quantum-confinement size, whereas photochemical etching decreases the absorption volume with significant reduction in quantum-confinement size. Before etching, CdSe nanorods yield very weak PL (QE = 0.7%) with a short lifetime ($\tau_{\text{eff}} = 0.55$ ns). Chemical etching quenches PL of nanorods (QE = 0.3%, $\tau_{\text{eff}} = 0.33$ ns) even after binary amine–phosphine passivation,²¹ whereas photochemical etching or combination of chemical and photochemical etching results in high QEs (36–56%) with $\tau_{\text{eff}} = 6$ –12 ns. High QEs from photochemical etching are in sharp contrast with the

Scheme 1. Anisotropic Chemical and Photochemical Etching of CdSe Nanocrystals in Chloromethane Solvents



previous report of only a few % QEs for CdSe nanorods.²⁵ Furthermore, photochemical etching significantly narrows the fwhm from 30–32 nm to 19–21 nm. The brightened emission with a narrow bandwidth suggests the promise of photochemical etching in producing highly luminescent, nearly single-sized nanorods with targeted optical properties.

XRD, XPS, and MS Analysis of Etching Products. To provide a better understanding of etching chemistry, we characterized nanocrystals and etching byproducts by XRD, XPS, and MS. Powder XRD patterns indicate the W crystal structure for CdSe nanorods (Figure 3a). Notably, the height of the (002) peak increases as the heights of the (100), (101), (110), and (112) peaks decrease, which is in line with XRD patterns of vertically aligned, self-assembled nanorods on a silicon wafer.²⁶ Such an alignment of nanorods is probably due to the loss of surface ligands on the side-walls of nanorods. The XPS spectra (Figure 3b) show the presence of cadmium,

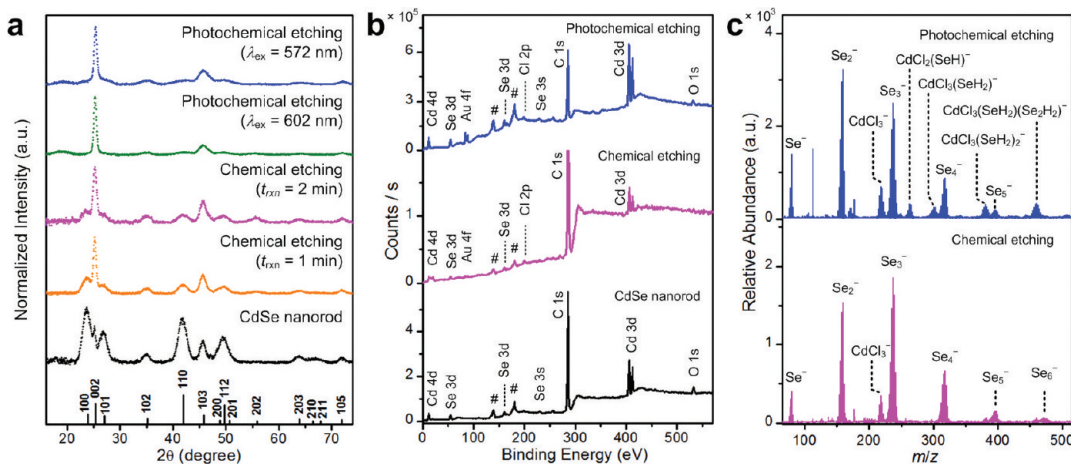


Figure 3. (a) XRD patterns of wurtzite CdSe nanorods before (black, bottom) and after chemical (orange and magenta, middle) and photochemical etching (olive and blue, top) in tetrachloromethane. Vertical lines represent the diffraction patterns for bulk CdSe. (b) XPS spectra of CdSe nanorods before (black) and after chemical (magenta) and photochemical etching (blue) in chloroform. Se Auger peaks are denoted by #. (c) Matrix-free laser desorption ionization mass spectra of the etching products obtained from chemical (magenta) or photochemical (blue) etching in chloroform. a.u., arbitrary unit.

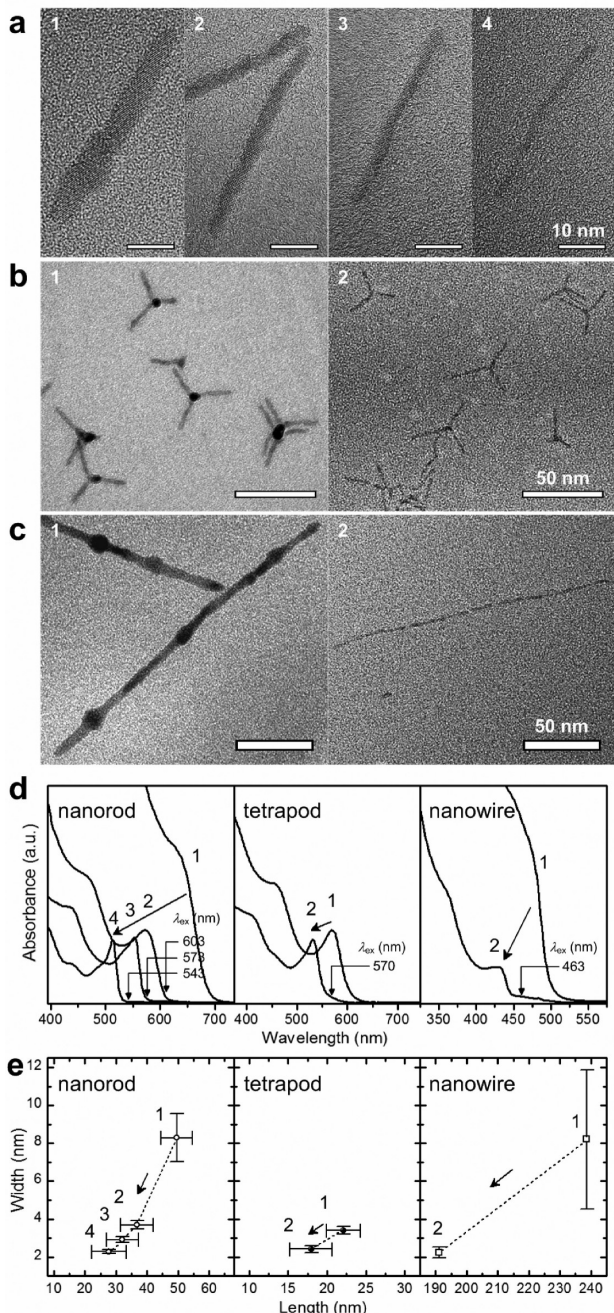


Figure 4. (a) TEM images of CdSe nanorods before (1) and after photochemical etchings for 330 min at $\lambda_{ex} = 603$ nm (2), for 90 min at 573 nm (3), and for 40 min at 543 nm (4). (b) TEM images of CdSe tetrapods before (1) and after photochemical etching for 95 min at 570 nm (2). (c) TEM images of CdS nanowires before (1) and after photochemical etching for 180 min at 463 nm (2). (d) Absorption spectra and (e) average widths and lengths of nanocrystal samples before and after photochemical etching. Inverted triangle denotes the excitation wavelength. Error bars represent the standard deviation.

selenium, carbon, and oxygen atoms on the surface of CdSe nanorods before and after etching. A strong carbon peak originates from organic ligands coordinated to the surface of nanocrystals.²¹ An oxygen peak indicates some oxidation of nanocrystals during sample preparation in air.²¹ Importantly, a chlorine peak appears in a trace amount after both chemical and photochemical etching, suggesting an active role of chlorine/chloride in both processes. The negative ion mass spectra of the

etching products (Figure 3c) show cadmium trichloride ($CdCl_3^-$) and a series of selenium clusters (Se_x^-) from both chemical and photochemical etching, as well as additional peaks containing both cadmium chloride and selenium hydride from photochemical etching. Peak assignments are given in Figure S2 of the Supporting Information. The positive ion mass spectra (data not shown) indicate the presence of tributylphosphine selenide in the etching product. MS results strongly suggest that the chloride ion attacks the electron-deficient cadmium atom on the surface of nanocrystals and forms cadmium chloride and TBP coordinates to electron-rich selenide on the surface to form tributylphosphine selenide, which is soluble in both chloroform and tetrachloromethane. Note that tributylphosphine selenide is typically formed in organic solvents by dissolving both TBP and selenium powder.²¹ Thus, a reverse equilibrium process would yield TBP and selenium clusters from tributylphosphine selenide. Photochemical etching differs from chemical etching in the pronounced height of peaks containing both cadmium chloride and selenium hydride.

Mechanism of Anisotropic Etching. Taking the structural and chemical analysis results together, we propose a mechanism of chemical and photochemical etching, as shown in Scheme 1.

Facet-Selective Chemical Etching. For chemical etching, organic-soluble nanocrystals were dissolved either in oxygen-free tetrachloromethane or in oxygen-saturated chloroform, both of which contained TBP as an additive. Addition of propylamine quenched chemical etching in both tetrachloromethane and chloroform solutions containing TBP.

The chloride ion is considered to be the active species, and the source of the chloride ion is chloromethane solvents. According to the literature,²⁷ tetrachloromethane reacts with TBP to yield tributyltrichloromethylphosphonium chloride ($[Bu_3P-CCl_3]^+Cl^-$) (Scheme 1 top i). However, chloroform does not react with TBP. In the presence of oxygen, TBP is oxidized to TBPO via TBP dioxygen diradical (Bu_3P-O-O).²⁸ This dioxygen diradical intermediate can induce the oxidation of chloroform to produce hydrochloric acid (HCl) (Scheme 1, top ii), similarly to photoinduced radical decomposition of chloroform.²⁹ Autoxidation of chloroform by oxygen is not considered here because commercial chloroform contains 0.5–1% ethanol as a preservative. Thus, the chloride ion is produced either by the reaction of tetrachloromethane with TBP in the absence of oxygen or by the oxidation of chloroform with TBP dioxygen diradical in the presence of oxygen.

Chemical etching almost exclusively erodes the end facets [(001)_W and (00-1)_W] of W nanorods (Scheme 1, top), suggesting that end planes are more susceptible to the chloride ion etching than side-walls. Strongly coordinating ligands such as phosphonic acids that stabilize the side-walls⁵ form a protective layer that could block the diffusion of chloride ions to the nanocrystal surface. Propylamine that coordinates cadmium atoms on the nanocrystal surface quenches the chemical etching by protecting surface cadmium atoms from the chloride ions, similarly to the inhibition of metal corosions by primary amines under acidic conditions.^{30,31} Other primary amines such as butylamine and octylamine also effectively quench the etching, just as in corrosion inhibition.^{30,31} The extent of chemical etching varies with the concentration of TBP as well as the reaction time (t_{rxn}). As the chemical etching proceeds, nanocrystals are aggregated in tetrachloromethane but not in chloroform. Because the absence or the presence of the side product TBPO was the key difference between the two

Table 3. Band-Edge Absorption Wavelength and the Average Size of CdSe Nanorods, CdSe Tetrapods, and CdSe Nanowires before and after Photochemical Etching Shown in Figure 4^a

	λ_{abs} (nm)	length (L , nm)	diameter(ϕ , nm)	aspect ratio ^b
CdSe nanorod	643	59.6 \pm 5.1	8.3 \pm 1.3	6.1 \pm 1.1
etching for 330 min at $\lambda_{\text{ex}} = 603$ nm	575	36.8 \pm 5.3	3.7 \pm 0.2	10.0 \pm 1.5
etching for 90 min at $\lambda_{\text{ex}} = 573$ nm	549	32.1 \pm 2.3	2.9 \pm 0.2	11.0 \pm 1.6
etching for 40 min at $\lambda_{\text{ex}} = 543$ nm	510	27.7 \pm 5.6	2.3 \pm 0.1	12.2 \pm 2.4
CdSe tetrapod	569	22.1 \pm 2.2	3.4 \pm 0.2	6.5 \pm 0.7
etching for 95 min at $\lambda_{\text{ex}} = 570$ nm	532	18.0 \pm 2.7	2.4 \pm 0.2	7.5 \pm 1.4
CdS nanowire	480	238.7 \pm 0.2	8.2 \pm 3.7	
etching for 180 min at $\lambda_{\text{ex}} = 463$ nm	427	191.1 \pm 0.2	2.2 \pm 0.3	

^aThe numbers of nanocrystal samples are 62 (CdSe nanorod before etching), 89 (CdSe nanorod after 603 nm photochemical etching), 46 (CdSe nanorod after 573 nm photochemical etching), 34 (CdSe nanorod after 543 nm photochemical etching), 30 (CdSe tetrapod before etching), and 30 (CdSe tetrapod after 570 nm photochemical etching). The number of points used to calculate the average width of a single CdS nanowire is 10 (before etching) and 12 (after 463 nm photochemical etching). The width is measured across the length of CdS nanowire at \sim 20 nm intervals. ^bAn error denotes the standard deviation.

solvent conditions, TOPO was added to the tetrachloromethane solution to prevent nanocrystals from aggregating.¹

Quantum Size-Selective Photochemical Etching. For photochemical etching, nanocrystals were dissolved in tetrachloromethane or chloroform containing both primary amine (either oleylamine or propylamine) and TBP as additives in the absence of oxygen. The active species in photochemical etching is also considered to be the chloride ion, because it can be produced by electron transfer from photoexcited nanocrystals to chloromethane adsorbed on the nanocrystal surface (Scheme 1, bottom). It has been previously reported that photodegradation of polystyrene occurs in chloromethane because of the chloride ion generated by the photoinduced electron transfer from styrene chromophore to chloromethane.³²

Photochemical etching preferentially erodes the side-walls of W nanorods (Scheme 1, bottom), indicating that the electron-transfer rate from nanocrystal to chloromethane is higher on the side-walls than the end facets because excitons are mostly localized in a plane perpendicular to the cylindrical axis of W nanorod.

Primary amine that quenches chemical etching facilitates photochemical etching by dissolving cadmium chloride from the nanocrystal surface into the solution in the form of dialkylamine cadmium chloride complexes.^{21,33} Addition of TBP increases the rate of photochemical etching. Nanocrystals are not aggregated during photochemical etching even in the absence of TBPO or TOPO because primary amine is a good coordinating ligand for cadmium.²¹ The extent of photochemical etching varied with the light-exposure time and photoexcitation wavelength (λ_{ex}).

Anisotropic Etching of Nanocrystal Tetrapods and Nanowires. Lastly, we applied chemical and photochemical etching to reshape CdSe tetrapods and W CdS nanowires. The ZB CdSe core/W CdSe arm tetrapod is grown over the (111)_{ZB} facets of the ZB core, and the (00−1)_W facet overlaps with (111)_{ZB}.⁷ Tetrapod has the (00−1)_W facet at the end of each pod, and the diameter of pod becomes the quantum-confinement size, similarly to nanorod. The CdS nanowire also has the W structure grown along the *c*-axis, and the exciton is radially confined. Results from photochemical etching are compared with those of CdSe nanorods in Figure 4. Variations in band-edge absorption and average size before and after photochemical etching are summarized in Table 3. Photochemical etching reduces the diameter of the four arms of CdSe tetrapods (Figure 4b) as well as the diameter of CdS nanowires

(Figure 4c), demonstrating the anisotropic etching of nanocrystals. On the other hand, chemical etching shortens the length only (data not shown). Notably, photochemical etching can easily reduce the diameter to less than 3 nm (Figure 4e), which has not been achieved by colloidal growth alone (see Figure S3 of the Supporting Information). Moreover, photochemical etching narrows down the distribution of quantum-confinement size (Figure 4e) and sharpens the band-edge absorption feature (Figure 4d). Remarkably, photochemical etching yields nearly single-sized nanorods, tetrapods, and nanowires.

A remarkable difference in anisotropy between the two etching processes suggests that the chemically generated chloride ion removes surface atoms almost exclusively from the (00±1)_W end faces, whereas the photoinduced chloride ion erodes surface atoms mostly from the side walls because the excited electron is leaked out more easily to the side walls than to the end faces. As a result, chemical etching becomes length-selective, whereas photochemical etching becomes diameter-selective. Besides, either chemical or photochemical generation of the chloride ion allows the easy, precise control over both start and stop of etching processes. Thus, it is now possible to finely tune the quantum-confinement size and aspect ratio of semiconductor nanorods, tetrapods, and nanowires by combination of colloidal growth and chemical/photochemical etching in organic solvents (see Figure S3 in the Supporting Information).

CONCLUSION

We report both chemical and photochemical etching in chloromethane solvents that are compatible with organic-based colloidal synthesis of semiconductor nanocrystals. As-synthesized CdSe nanorods and tetrapods, as well as CdS nanowires, can be reshaped either by the facet-selective chemical etching or by the quantum-size-selective photochemical etching. Chemical etching shortens the length, whereas photochemical etching reduces the diameter. The etching processes are initiated/terminated by addition of TBP/propylamine in chemical etching and by turning the excitation light on/off in photochemical etching. Both chemical and photochemical etching can be sequentially combined together with colloidal growths to reproducibly prepare single-diameter anisotropic nanocrystals emitting at the targeted wavelength. The present etching method, which employs the reactive chloride ion in combination with chalcogen-coordinating

trialkylphosphine and metal-coordinating primary amine, is applicable to anisotropic etching of other compound semiconductor nanocrystals in organic solvent.

■ ASSOCIATED CONTENT

§ Supporting Information

Results of etching in chloroform, mass spectra and peak assignments, size distribution of nanocrystals, and fitting parameters for PL decay. This material is available free of charge via the Internet at <http://pubs.acs.org>.

■ AUTHOR INFORMATION

Corresponding Author

*E-mail: skshin@postech.ac.kr.

■ ACKNOWLEDGMENTS

S.J.L. and J.S. acknowledge the postdoctoral support from the Brain Korea 21 program administered by the Ministry of Education, Science and Technology (MEST). We are thankful for the support from the Nano Research and Development Program through the National Research Foundation of Korea funded by MEST (Grant No. 2010-0019151) and the Advanced Scientific Analysis Instruments Development Project administered by the Korean Research Institute of Standards and Science.

■ REFERENCES

- (1) Murray, C. B.; Norris, D. J.; Bawendi, M. G. *J. Am. Chem. Soc.* **1993**, *115*, 8706–8715.
- (2) Yu, W. W.; Qu, L.; Guo, W.; Peng, X. *Chem. Mater.* **2003**, *15*, 2854–2860.
- (3) Peng, X.; Manna, L.; Yang, W.; Wickham, J.; Scher, E.; Kadavanich, A.; Alivisatos, A. P. *Nature* **2000**, *404*, 59–61.
- (4) Li, L.; Hu, J.; Yang, W.; Alivisatos, A. P. *Nano Lett.* **2001**, *1*, 349–351.
- (5) Peng, Z. A.; Peng, X. *J. Am. Chem. Soc.* **2002**, *124*, 3343–3353.
- (6) Yu, H.; Li, J.; Loomis, R. A.; Gibbons, P. C.; Wang, L. -W.; Buhro, W. E. *J. Am. Chem. Soc.* **2003**, *125*, 16168–16169.
- (7) Manna, L.; Milliron, D. J.; Meisel, A.; Scher, E. C.; Alivisatos, A. P. *Nat. Mater.* **2003**, *2*, 382–385.
- (8) Asokan, S.; Krueger, K. M.; Colvin, V. L.; Wong, M. S. *Small* **2007**, *3*, 1164–1169.
- (9) Rogach, A. L.; Gaponik, N.; Lupton, J. M.; Bertoni, C.; Gallardo, D. E.; Dunn, S.; Pira, N. L.; Paderi, M.; Repetto, P.; Romanov, S. G.; O'Dwyer, C.; Torres, C. M. S.; Eychmüller, A. *Angew. Chem., Int. Ed.* **2008**, *47*, 6538–6549.
- (10) Hillhouse, H. W.; Beard, M. C. *Curr. Opin. Colloid Interface Sci.* **2009**, *14*, 245–259.
- (11) Liu, L.; Peng, Q.; Li, Y. *Inorg. Chem.* **2008**, *47*, 5022–5028.
- (12) Liu, J.; Yang, X.; Wang, K.; Wang, D.; Zhang, P. *Chem. Commun.* **2009**, 6080–6082.
- (13) Liu, J.; Araguete, D. M.; Jinschek, J. R.; Rimstidt, J. D.; Hochella, M. F. Jr. *Geochim. Cosmochim. Acta* **2008**, *72*, 5984–5996.
- (14) Li, R.; Lee, J.; Yang, B.; Horspool, D. N.; Aindow, M.; Papadimitrakopoulos, F. *J. Am. Chem. Soc.* **2005**, *127*, 2524–2532.
- (15) Matsumoto, H.; Sakata, T.; Mori, H.; Yoneyama, H. *J. Phys. Chem.* **1996**, *100*, 13781–13785.
- (16) Torimoto, T.; Murakami, S.; Sakuraoka, M.; Iwasaki, K.; Okazaki, K.; Shibayama, T.; Ohtani, B. *J. Phys. Chem. B* **2006**, *110*, 13314–13318.
- (17) Uematsu, T.; Kitajima, H.; Kohma, T.; Torimoto, T.; Tachibana, Y.; Kuwabata, S. *Nanotechnology* **2009**, *20*, 215302.
- (18) Torimoto, T.; Hashitani, M.; Konishi, T.; Okazaki, K.; Shibayama, T.; Ohtani, B. *J. Nanosci. Nanotech.* **2009**, *9*, 506–513.
- (19) Galian, R. E.; de la Guardia, M.; Pérez-Prieto, J. *J. Am. Chem. Soc.* **2009**, *131*, 892–893.
- (20) Talapin, D. V.; Gaponik, N.; Borchert, H.; Rogach, A. L.; Haase, M.; Weller, H. *J. Phys. Chem. B* **2002**, *106*, 12659–12663.
- (21) Kim, W.; Lim, S. J.; Jung, S.; Shin, S. K. *J. Phys. Chem. C* **2010**, *114*, 1539–1546.
- (22) Deprèle, S.; Montchamp, J.-L. *J. Org. Chem.* **2001**, *66*, 6745–6755.
- (23) Xi, L.; Lam, Y. M. *Chem. Mater.* **2009**, *21*, 3710–3718.
- (24) Robinson, R. D.; Sadler, B.; Demchenko, D. O.; Erdonmez, C. K.; Wang, L. -W.; Alivisatos, A. P. *Science* **2007**, *317*, 355–358.
- (25) Manna, L.; Scher, E. C.; Li, L.-S.; Alivisatos, A. P. *J. Am. Chem. Soc.* **2002**, *124*, 7136–7145.
- (26) Zanella, M.; Gomes, R.; Povia, M.; Giannini, C.; Zhang, Y.; Riskin, A.; Van Bael, M.; Hens, Z.; Manna, L. *Adv. Mater.* **2011**, *23*, 2205–2209.
- (27) Lorca, M.; Kurosu, M. *Synth. Commun.* **2001**, *31*, 469–473.
- (28) Burkett, H. D.; Hill, W. E.; Worley, S. D. *Phosphorus Sulfur Relat. Elem.* **1984**, *20*, 169–172.
- (29) Cohen, L. R.; Peña, L. A.; Seidl, A. J.; Olsen, J. M.; Wekselbaum, J.; Hoggard, P. E. *Monatsh. Chem.* **2009**, *140*, 1159–1165.
- (30) de Damborenea, J.; Bastidas, J. M.; Vazquez, A. J. *Electrochim. Acta* **1997**, *42*, 455–459.
- (31) Feng, Y.; Chen, S.; You, J.; Guo, W. *Electrochim. Acta* **2007**, *53*, 1743–1753.
- (32) Bortolus, P.; Minto, F.; Lora, S.; Gleria, M.; Beggiato, G. *Polym. Photochem.* **1984**, *4*, 45–57.
- (33) Broome, F. K.; Ralston, A. W.; Thornton, M. H. *J. Am. Chem. Soc.* **1946**, *68*, 67–69.